ACS Catalysis

Letter

Cite This: ACS Catal. 2020, 10, 1417−1422

pubs.acs.org/acscatalysis

In Situ Monitoring of Heterogeneous Catalytic Hydrogenation via ^{129}Xe NMR Spectroscopy and Proton MRI

Dudari B. Burueva,[†,§,#] Ekaterina V. Pokochueva,[†,§,#] Xinpei Wang,[‡,⊥] Max Filkins,[∥,⊥] Alexandra Svyatova,[†,§] Sean P. Rigby,[∥] Chengbo Wang,[‡] Galina E. Pavlovskaya,[⊥,▽] Kirill V. Kovtunov,[*,†,§] Thomas Meersmann,[*,⊥,▽] and Igor V. Koptyug[†,§]

[†]International Tomography Center SB RAS, 3A Institutskaya St., 630090 Novosibirsk, Russia

[§]Novosibirsk State University, 2 Pirogova St., 630090 Novosibirsk, Russia

[‡]Faculty of Science and Engineering, University of Nottingham Ningbo China, 199 Taikang East RD, Ningbo 315100, China

[∥]Department of Chemical and Environmental Engineering, University of Nottingham, Nottingham NG7 2RD, United Kingdom

[⊥]Sir Peter Mansfield Imaging Centre, University of Nottingham, Nottingham NG7 2RD, United Kingdom

[▽]Division of Respiratory Medicine, School of Medicine, University of Nottingham, Nottingham NG7 2HU, United Kingdom

Supporting Information

ABSTRACT: The ability to use molecular hydrogen, H_2, as a buffer gas in spin exchange optical pumping of noble gases enables the production of hydrogen gas containing a low percentile (5%) of hyperpolarized (HP) ^{129}Xe as a tracer for in situ NMR spectroscopy of hydrogenation reactions. It is demonstrated that the xenon chemical shift, observed in the porous space of Pt-containing alumina pellets, can be used to monitor the temperature changes under rapidly progressing, nonsteady-state conditions during start-up of the catalytic reaction. Standard proton MR imaging was successfully applied to provide in situ evaluation of conversion for the catalyst used in this work.

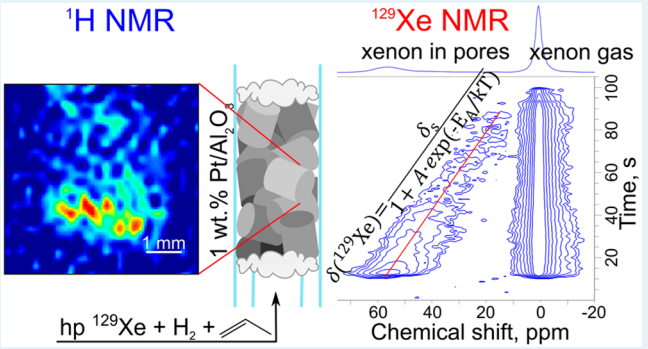

KEYWORDS: *NMR thermometry, heterogeneous hydrogenation, hyperpolarization, xenon, parahydrogen*

The vast majority of contemporary, industrially relevant, chemical processes are catalytic, and heterogeneous catalytic reactions are of particular interest.[1] To optimize the activity and selectivity of catalytic reaction, the comprehensive evaluation of reaction parameters is essential. Magnetic resonance methods, that is, nuclear magnetic resonance spectroscopy (NMR) and magnetic resonance imaging (MRI), are powerful instruments to do so. Because of their noninvasive nature, NMR and MRI can be used for operando studies of catalytic reactions;[2,3] for instance, these techniques can be successfully used for obtaining spatially resolved conversion information[4−7] and velocity distributions[8−11] for catalytic reactors, for monitoring the process of catalyst preparation,[12−14] and even for temperature measurements. NMR thermometry of working catalytic reactors is based on the temperature dependence of the properties that can be measured by NMR, such as the chemical shift,[7,15] the NMR signal width,[16] or the NMR signal intensity.[17,18] It either utilizes external substances with temperature-sensitive NMR properties (such as ethylene glycol in a capsule[7,15]), or relies on the properties of the NMR signals of the catalysts (e.g., ^{27}Al NMR spectroscopy of alumina[17,18]) or the reactants themselves. Successful measurements based on the NMR detection of external inserts placed inside the catalytic reactor have been reported that do not lead to magnetic field distortions. However, in some cases the temperature readout may be misinterpreted, because NMR parameters mentioned above depend not only on temperature, but on other experimental factors as well—including the amount of a substance used for temperature evaluation, diffusion effects, and spectral resolution.[19] Even the methods that are based on direct magnetic resonance measurements of the reactants and products may impose certain restrictions on the experimental design; for instance, the use of NMR line width for temperature evaluation precludes the use of a frequency encoding gradient for MRI.[16] Furthermore, on a catalytic surface it may be difficult to differentiate between the surface temperature and that of the fluid phase. Perhaps most importantly, MR methods generally suffer from low sensitivity, which may cause prolonged acquisition times and may prevent the time-resolved study of nonsteady-state processes. The MRI sensitivity problem in heterogeneous catalysis is further

Received: November 18, 2019
Revised: December 29, 2019
Published: December 30, 2019

DOI: 10.1021/acscatal.9b05000
ACS Catal. 2020, 10, 1417−1422

exacerbated by magnetic field inhomogeneity at the surface of solid catalysts beads and within the entire catalytic reactor.[4] Furthermore, industrial catalytic processes are often subjected to high temperatures[1,20] – meaning that many catalytic reactions usually proceed in the gaseous phase so that, even at elevated pressures, the spin density is substantially reduced compared with the condensed phase.[19]

To overcome these obstacles, hyperpolarization methods[21,22] or remote detection techniques[23,24] can be applied. The hyperpolarization methods are of particular interest—including spin-exchange optical pumping (SEOP)[25] and parahydrogen-induced polarization (PHIP),[26,27] which provide a significant increase in NMR signals intensity, by up to several orders of magnitude.

The SEOP technique allows for the production of hyperpolarized (HP) noble gases, such as HP ^{3}He, HP ^{129}Xe, HP ^{131}Xe, and HP ^{83}Kr, via spin-exchange with the electronically spin-polarized alkali metal atoms, which have absorbed circularly polarized resonance light.[28,29] Among all NMR active isotopes of noble gases, ^{129}Xe is particularly interesting because the chemical shift of xenon is extremely sensitive to the external conditions—the chemical shift range of xenon in different environments is over 200 ppm wide.[30] This property, combined with xenon chemical inertness and absence of background signals, has made xenon, hyperpolarized by SEOP, an ideal magnetic resonance probe of pore sizes for high-surface-area materials like aerogel, alumina, and zeolites.[31−37] Generally, adsorption processes and host−guest interactions in porous materials can be followed and analyzed by ^{129}Xe NMR spectroscopy.[38−40] Furthermore, HP ^{129}Xe has been used in high-temperature MRI studies as a tracer gas for methane combustion, demonstrating that the hyperpolarized spin state of the noble gas nuclei can survive extreme temperature conditions and that imaging of the combustion region at a very low spin temperature is feasible.[41] An uninterrupted supply of methane gas containing 5% of HP ^{129}Xe can be obtained directly under continuous flow conditions provided that about 5−10% of N_2 is added to the gas mixture as a radiation quenching agent for the SEOP process. Of particular promise is that no N_2 is required to generate HP ^{129}Xe if molecular hydrogen is used as a buffer gas for the SEOP process, enabling the production of a supply of H_2 containing a small percentile of HP ^{129}Xe as a tracer gas.[42]

^{129}Xe NMR spectroscopy can be used for temperature studies as well−temperature dependence of xenon chemical shift has been studied in various systems, such as pure Xe gas,[43] Xe dissolved in water,[44] *n*-alkanes,[45] or other organic solvents,[46] encapsulated Xe (e.g., Xe in cryptophane-A cage[46,47]) and Xe adsorbed on the surface of various porous materials.[48,49] For different systems, temperature dependence may vary significantly and be either linear or nonlinear. For example, several models have been developed for the temperature dependence of the chemical shift for xenon adsorbed in zeolites. The most suitable for experimental use is that described by Cheung[48] which may be represented as

$$\delta(T) = \frac{c|\varepsilon|}{1 + Ae^{-\varepsilon/kT}}$$

where ε is the depth of square-well potential (used for describing Xe-porous media interactions), c is a phenomenological constant, A is a geometric term dependent on xenon's van der Waals radius and morphology of pores, k is the Boltzmann constant, and T is the temperature.

Pronounced temperature dependence allows xenon to be used as a temperature probe for biomedical applications—although xenon atoms are not included in any biologically active molecules.[50] For instance, the applicability of lipid-dissolved hyperpolarized xenon gas for absolute MR temperature measurements (including in vivo experiments[51,52]) has been shown for the examples of white[51] and brown adipose tissue,[52] and neat triglycerides.[53] However, to date, no direct in situ temperature measurements of chemical reactions have been performed.

Parahydrogen-induced polarization (PHIP), another hyperpolarization technique, is based upon catalytic hydrogenation with parahydrogen (p-H_2).[54,55] If the hydrogenation proceeds via pairwise hydrogen addition route (i.e., the two H atoms from the same p-H_2 molecule end up in the same product molecule), the corresponding ^{1}H NMR signals of reaction products or intermediates can be significantly enhanced, exhibiting characteristic antiphase lineshapes.[56] As a result, the appearance of antiphase signals in the ^{1}H NMR spectrum indicates the positions in the product molecules or reaction intermediates to which H atoms were added. PHIP was also proven to be very useful for mechanistic investigations in both homogeneous[57,58] and heterogeneous catalysis.[59−62] Gases hyperpolarized by PHIP (for example, hyperpolarized propane formed in propene hydrogenation with parahydrogen) were also successfully used for MR visualization of void spaces of model objects[63−65] as well as for MRI of working catalytic reactors.[11,66]

In this study, we demonstrate the potential for temperature-dependent HP ^{129}Xe NMR spectra coupled with proton MR imaging as an in situ measurement technique for catalytic processes. First, the temperature dependence of the chemical shift for xenon in catalyst pores was studied—see Supporting Information for further details. Briefly, ^{129}Xe NMR spectra were obtained for xenon adsorbed in pores of 1 wt % Pt/Al_2O_3 pellet with an eggshell catalyst distribution (Figure S1) under ambient pressure while HP xenon mixture (5 vol % Xe in natural abundance, 95 vol % N_2) was flowing. The cylindrical pellet of size 3.2 mm was located at the bottom of a 10 mm NMR tube and outgassed for several hours at 150 °C in a vacuum before the introduction of HP xenon. Also, before the exposure of the pretreated pellet to HP xenon, propene gas was added to the pellet. The sample in the coil was equilibrated for at least 5 min at each temperature before data acquisition began. The chemical shift of the resonance corresponding to the xenon in the pores is displayed as a function of temperature in Figure S2. For the xenon adsorbed in catalyst pores, the chemical shift decreases as the temperature increases. Following the model described by Cheung,[48] the temperature dependence of the xenon chemical shift can be rewritten as

$$\delta_{129_{Xe}} = \frac{\delta_s}{1 + Ae^{-E_A/kT}}$$

where E_A is the surface adsorption energy and δ_s is the "true" chemical shift of xenon on the surface. This equation assumes that the chemical shift of gas phase xenon, in the limit of zero density, is set to 0 ppm.

The experimental data are well approximated by this equation (Figure S2). The δ_s value is taken as 145 ppm based on the study by Filimonova et al.,[67] where this chemical shift was found for xenon adsorbed on the surface of 2% Pt/

DOI: 10.1021/acscatal.9b05000
ACS Catal. 2020, 10, 1417−1422

Al_2O_3 catalyst at −50 °C. It should be noted that the chemical shift of free xenon gas does not depend upon temperature over this temperature range. No temperature hysteresis was found.

The temperature dependence of the ^{129}Xe chemical shift and the capability to generate HP ^{129}Xe through SEOP of a 0.05:0.95 Xe:H_2 gas mixture was utilized to observe a catalytic reaction during start-up with time-resolved ^{129}Xe NMR spectroscopy (using 99% isotopically enriched ^{129}Xe). After SEOP, the HP ^{129}Xe:H_2 gas was mixed under continuous flow conditions with propene in a 2:1 ratio and then directed into a catalytic reactor (8.5 mm ID quartz tube packed with 15 cylindrical Pt/Al_2O_3 pellets, two outer cooling jackets were used). A schematic diagram of the catalytic reactor is presented in Figure S3. It is expected that after the contact of the propene:H_2:Xe mixture with the catalyst pellets, propene and hydrogen start to react with each other producing propane, and heat is released in the highly exothermic propene hydrogenation reaction. Therefore, the actual temperature of the catalyst pellet may be significantly higher than the value which a downstream thermocouple temperature probe would display.

Time-resolved ^{129}Xe chemical shift data were obtained by acquiring single-scan NMR spectra following a 90° rf excitation pulse, recorded once per second while the propene:H_2:Xe mixture was flowing continuously (Figure 1). Gas flow was

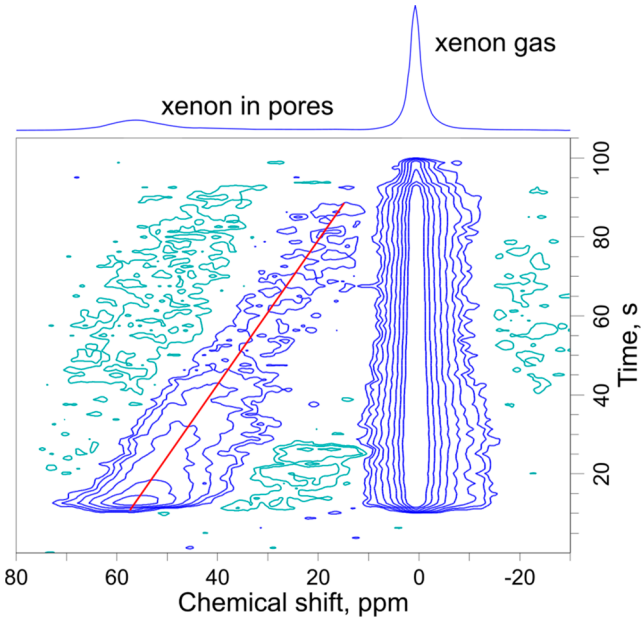

Figure 1. ^{129}Xe NMR spectra of catalytic reactor packed with Pt/Al_2O_3 pellets while propene:H_2:Xe mixture was flowing continuously. The gas flow reaches the reactor at about 10 s which shows the starting conditions with 56 ppm for xenon in the material phase. As the catalytic reaction progressively increases the surface temperature, the NMR signal is shifted (the red line serving as a guidance to the eyes).

initiated, and the xenon signal appeared about 10 s into the acquisition, when the gas stream arrived at the NMR detection cell. The ^{129}Xe chemical shift from the materials phase decreased significantly over the next 80 s, while the changes in the chemical shift of gaseous xenon, if any, remained below the observed spectral resolution. Taking into account the temperature dependence of xenon chemical shift obtained in the calibration experiments, the average temperature inside the catalytic reactor was about 106 °C within 30 s after the start of the reaction and increased to about 200 °C within 70 s. However, the temperature inside the reactor measured with a thermocouple in a separate experiment did not exceed 150 °C. Such a significant difference in temperature values can be explained by the fact that the noninvasiveness cannot be guaranteed when using the thermocouple. Moreover, the fast temperature increase due to the exothermic reaction is taking place in the thin outer layer of the pellet, where platinum particles are located and where xenon is adsorbed, making the thermocouple measurement uninformative.

It is also noted that, although the presence of H_2 can significantly alter the chemical shift of xenon adsorbed on platinum surfaces,[38,39] no such observation was made in this study in the presence of propene with the pellets used in this work. The ambient temperature chemical shift observed with the Xe:N_2 mixture was almost identical to the one measured at the beginning of the reaction with Xe:H_2:propene described below.

Besides ^{129}Xe NMR spectroscopy, standard proton MRI studies of the Pt/Al_2O_3 pellet during propene hydrogenation were performed using an ultrashort TE (UTE)[68] pulse sequence with selective propane/propene signal suppression. Selective suppression works in a following way. A selective rf pulse tuned to the propene (propane) resonance frequency saturates propene (propane) protons, leaving only propane (propene) protons to produce a signal.

In addition to standard proton MRI, the use of hyperpolarized ^{1}H MRI through parahydrogen could be useful for in situ monitoring of the catalytic reaction. The enhanced MR signals produced via PHIP could significantly shorten the data acquisition time. However, in this work, the advantage of using parahydrogen instead of normal hydrogen (thermally equilibrated hydrogen with the ratio of ortho- and para-isomers approaching 3:1 at 298 K) in propene hydrogenation over commercially available 1 wt % Pt/Al_2O_3 is limited by a 2-fold NMR signal enhancement only because of the low contribution of the pairwise hydrogen addition over the pellets of Pt/Al_2O_3 catalyst (Figure S4). For hyperpolarized ^{1}H MR imaging, special MRI-compatible catalytic systems can be designed that provide high NMR signal enhancements due to high contribution of pairwise hydrogen addition and minimize distortions arising from field inhomogeneity.[66]

The optimization of parameters for the UTE imaging with selective suppression of ^{1}H signals from either propane or propene was performed by using a 10 mm OD NMR tube filled with propene gas concentrically placed inside a 15 mm OD NMR tube filled with propane gas (Figure S5). After optimization, the parameters were as follows: the selective 90° pulse for the suppression of ^{1}H signals of propane gas had a Gaussian shape with 1000 Hz bandwidth and 320 Hz frequency offset; in the case of selective propene signal suppression, the selective 90° pulse had a Gaussian shape with 2000 Hz bandwidth and 1000 Hz frequency offset. The MR images with/without selective suppression of propene signals of 1 wt % Pt/Al_2O_3 pellet placed at the bottom of 5 mm NMR tube and flushed with propene are presented in Figure S6.

Further, MR images with selective suppression of ^{1}H signals from either propane or propene during propene hydrogenation with normal hydrogen over the 1 wt % Pt/Al_2O_3 catalyst pellet placed at the bottom of a 5 mm NMR tube were acquired (Figure 2). The propene:H_2 mixture was supplied from the top to the bottom. The fact that selective suppression of the

DOI: 10.1021/acscatal.9b05000
ACS Catal. 2020, 10, 1417−1422

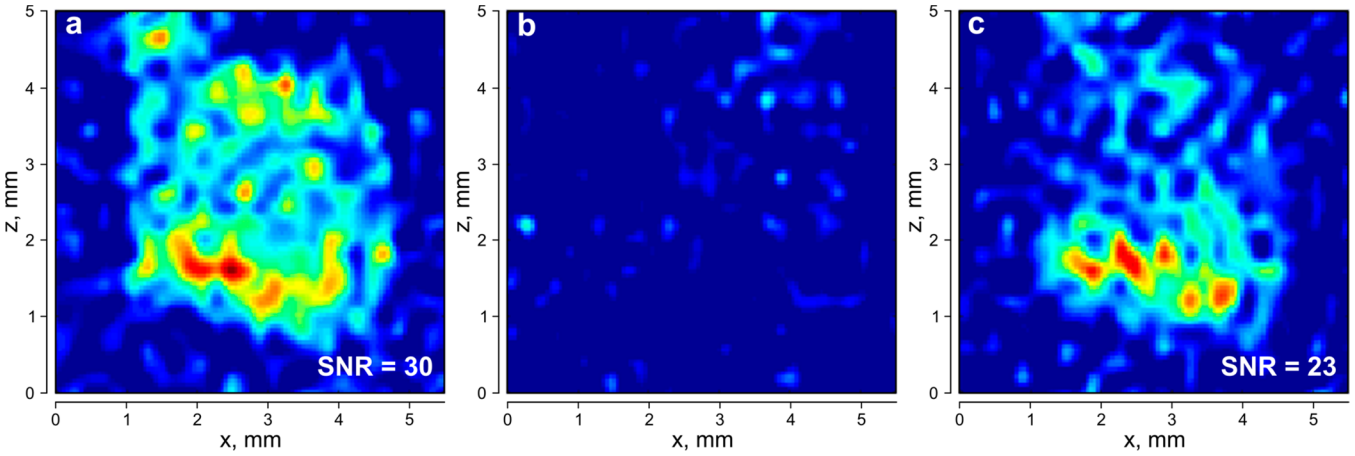

Figure 2. ^{1}H UTE MR images of a single Pt/Al_2O_3 pellet placed at the bottom of 5 mm NMR tube (a) without any suppression pulse; (b) with propane signals suppression pulse; (c) with propene signals suppression pulse. MR images were acquired during propene hydrogenation with normal hydrogen over 1 wt % Pt/Al_2O_3 catalyst pellet while the propene: n-H_2 mixture was flowing with the flow rate of 2.1 mL/s. All images have a pixel size of 0.0195 × 0.0195 cm^2 and were acquired with the repetition time of 40 ms. Number of averages = 64.

propane resonance leads to an almost complete absence of signal in the MR image (Figure 2b) implies almost complete propene conversion over the Pt/Al_2O_3 pellet. In addition, the MR image with selective suppression of propene signal (Figure 2c) indicates that most of the propane is formed, and the heat is released, at the bottom part of the pellet, indicating the presence of temperature gradients, which cannot be measured by proton NMR.

In conclusion, it is demonstrated that HP ^{129}Xe NMR spectroscopy can be applied to time-resolved in situ temperature measurements of a working catalytic reactor under rapidly progressing, nonsteady-state conditions during reactor start-up. The ability to directly hyperpolarize ^{129}Xe within a 0.05:0.95 Xe:H_2 mixture greatly facilitates its usage for the study of hydrogenation reactions. The standard proton MR imaging under steady state conditions demonstrated that the propene hydrogenation conversion is close to 100% for the gas that reaches the catalyst pellet.

■ ASSOCIATED CONTENT

Supporting Information

The Supporting Information is available free of charge at https://pubs.acs.org/doi/10.1021/acscatal.9b05000.

Experimental section and supplement figures (PDF)

■ AUTHOR INFORMATION

Corresponding Authors

*E-mail: kovtunov@tomo.nsc.ru.

*E-mail: Thomas.Meersmann@nottingham.ac.uk.

ORCID

Sean P. Rigby: 0000-0002-2635-3416

Kirill V. Kovtunov: 0000-0001-7577-9619

Igor V. Koptyug: 0000-0003-3480-7649

Author Contributions

#(D.B.B., E.V.P.) These authors contributed equally.

Funding

Russian Science Foundation; British Council Researcher Links Grant Agreement 2017-RLWK9-11351

Notes

The authors declare no competing financial interest.

■ ACKNOWLEDGMENTS

The Russian team thanks RSF (grant no. 19-13-00047) for the support of MRI studies of hydrogenation reaction, and Russian Ministry of Science and Higher Education (AAAA-A16-116121510087-5) for the access to NMR/MRI equipment. This work was supported by the Engineering and Physical Sciences Research Council (EPSRC) [grant no. EP/R513283/1].

■ REFERENCES

(1) Lloyd, L. Industrial Catalysts. *Handbook of Industrial Catalysts. Fundamental and Applied Catalysis*; Springer: Boston, MA, 2011; pp 1−22.

(2) Koptyug, I. V. Magnetic Resonance Imaging Methods in Heterogeneous Catalysis. In *Spectroscopic Properties of Inorganic and Organometallic Compounds*; Yarwood, J., Douthwaite, R., Duckett, S., Eds.; The Royal Society of Chemistry: London, U.K., 2014; Vol. *45*, pp 1−42.

(3) Svyatova, A. I.; Kovtunov, K. V.; Koptyug, I. V. Magnetic Resonance Imaging of Catalytically Relevant Processes. *Rev. Chem. Eng.* **2019**, DOI: 10.1515/revce-2018-0035.

(4) Roberts, S. T.; Renshaw, M. P.; Lutecki, M.; McGregor, J.; Sederman, A. J.; Mantle, M. D.; Gladden, L. F. Operando Magnetic Resonance: Monitoring the Evolution of Conversion and Product Distribution during the Heterogeneous Catalytic Ethene Oligomerisation Reaction. *Chem. Commun.* **2013**, *49*, 10519−10521.

(5) Baker, L.; Renshaw, M. P.; Mantle, M. D.; Sederman, A. J.; Wain, A. J.; Gladden, L. F. Operando Magnetic Resonance Studies of Phase Behaviour and Oligomer Accumulation within Catalyst Pores during Heterogeneous Catalytic Ethene Oligomerization. *Appl. Catal., A* **2018**, *557*, 125−134.

(6) Ulpts, J.; Dreher, W.; Kiewidt, L.; Schubert, M.; Thöming, J. In Situ Analysis of Gas Phase Reaction Processes within Monolithic Catalyst Supports by Applying NMR Imaging Methods. *Catal. Today* **2016**, *273*, 91−98.

(7) Ulpts, J.; Kiewidt, L.; Dreher, W.; Thöming, J. 3D Characterization of Gas Phase Reactors with Regularly and Irregularly Structured Monolithic Catalysts by NMR Imaging and Modeling. *Catal. Today* **2018**, *310*, 176−186.

(8) Gladden, L. F. Magnetic Resonance in Reaction Engineering: Beyond Spectroscopy. *Curr. Opin. Chem. Eng.* **2013**, *2*, 331−337.

(9) Ren, X.; Stapf, S.; Blümich, B. NMR Velocimetry of Flow in Model Fixed-Bed Reactors of Low Aspect Ratio. *AIChE J.* **2005**, *51*, 392−405.

DOI: 10.1021/acscatal.9b05000
ACS Catal. 2020, 10, 1417−1422

(10) Lysova, A. A.; von Garnier, A.; Hardy, E. H.; Reimert, R.; Koptyug, I. V. The Influence of an Exothermic Reaction on the Spatial Distribution of the Liquid Phase in a Trickle Bed Reactor: Direct Evidence Provided by NMR Imaging. *Chem. Eng. J.* **2011**, *173*, 552−563.
(11) Bouchard, L.-S.; Burt, S. R.; Anwar, M. S.; Kovtunov, K. V.; Koptyug, I. V.; Pines, A. NMR Imaging of Catalytic Hydrogenation in Microreactors with the Use of Para-Hydrogen. *Science* **2008**, *319*, 442−445.
(12) Lysova, A. A.; Koptyug, I. V.; Sagdeev, R. Z.; Parmon, V. N.; Bergwerff, J. A.; Weckhuysen, B. M. Noninvasive in Situ Visualization of Supported Catalyst Preparations Using Multinuclear Magnetic Resonance Imaging. *J. Am. Chem. Soc.* **2005**, *127*, 11916−11917.
(13) Bergwerff, J. A.; Lysova, A. A.; Espinosa-Alonso, L.; Koptyug, I. V.; Weckhuysen, B. M. Monitoring Transport Phenomena of Paramagnetic Metal-Ion Complexes inside Catalyst Bodies with Magnetic Resonance Imaging. *Chem. - Eur. J.* **2008**, *14*, 2363−2374.
(14) Lysova, A. A.; Bergwerff, J. A.; Espinosa-Alonso, L.; Weckhuysen, B. M.; Koptyug, I. V. Magnetic Resonance Imaging as an Emerging Tool for Studying the Preparation of Supported Catalysts. *Appl. Catal., A* **2010**, *374*, 126−136.
(15) Gladden, L. F.; Abegão, F. J. R.; Dunckley, C. P.; Holland, D. J.; Sankey, M. H.; Sederman, A. J. MRI: Operando Measurements of Temperature, Hydrodynamics and Local Reaction Rate in a Heterogeneous Catalytic Reactor. *Catal. Today* **2010**, *155*, 157−163.
(16) Jarenwattananon, N. N.; Glöggler, S.; Otto, T.; Melkonian, A.; Morris, W.; Burt, S. R.; Yaghi, O. M.; Bouchard, L.-S. Thermal Maps of Gases in Heterogeneous Reactions. *Nature* **2013**, *502*, 537−540.
(17) Koptyug, I. V.; Khomichev, A. V.; Lysova, A. A.; Sagdeev, R. Z. Spatially Resolved NMR Thermometry of an Operating Fixed-Bed Catalytic Reactor. *J. Am. Chem. Soc.* **2008**, *130*, 10452−10453.
(18) Koptyug, I. V.; Sagdeev, D. R.; Gerkema, E.; Van As, H.; Sagdeev, R. Z. Solid-State 27Al MRI and NMR Thermometry for Catalytic Applications with Conventional (Liquids) MRI Instrumentation and Techniques. *J. Magn. Reson.* **2005**, *175*, 21−29.
(19) Zhivonitko, V. V.; Svyatova, A. I.; Kovtunov, K. V.; Koptyug, I. V. Recent MRI Studies on Heterogeneous Catalysis. *Annu. Rep. NMR Spectrosc.* **2018**, *95*, 83−145.
(20) Maegawa, T.; Akashi, A.; Yaguchi, K.; Iwasaki, Y.; Shigetsura, M.; Monguchi, Y.; Sajiki, H. Efficient and Practical Arene Hydrogenation by Heterogeneous Catalysts under Mild Conditions. *Chem. - Eur. J.* **2009**, *15*, 6953−6963.
(21) Kovtunov, K. V.; Pokochueva, E. V.; Salnikov, O. G.; Cousin, S. F.; Kurzbach, D.; Vuichoud, B.; Jannin, S.; Chekmenev, E. Y.; Goodson, B. M.; Barskiy, D. A.; Koptyug, I. V. Hyperpolarized NMR Spectroscopy: d-DNP, PHIP, and SABRE Techniques. *Chem. - Asian J.* **2018**, *13*, 1857−1871.
(22) Nikolaou, P.; Goodson, B. M.; Chekmenev, E. Y. NMR Hyperpolarization Techniques for Biomedicine. *Chem. - Eur. J.* **2015**, *21*, 3156−3166.
(23) Seeley, J. A.; Han, S.-I.; Pines, A. Remotely Detected High-Field MRI of Porous Samples. *J. Magn. Reson.* **2004**, *167*, 282−290.
(24) Zhivonitko, V. V.; Telkki, V.-V.; Koptyug, I. V. Characterization of Microfluidic Gas Reactors Using Remote-Detection MRI and Parahydrogen-Induced Polarization. *Angew. Chem., Int. Ed.* **2012**, *51*, 8054−8058.
(25) Walker, T. G.; Happer, W. Spin-Exchange Optical Pumping of Noble-Gas Nuclei. *Rev. Mod. Phys.* **1997**, *69*, 629−642.
(26) Kovtunov, K. V.; Zhivonitko, V. V.; Skovpin, I. V.; Barskiy, D. A.; Koptyug, I. V. Parahydrogen-Induced Polarization in Heterogeneous Catalytic Processes. In *Hyperpolarization Methods in NMR Spectroscopy*; Kuhn, L. T., Ed.; Springer-Verlag: Berlin, 2013; pp 123−180.
(27) Bowers, C. R. Sensitivity Enhancement Utilizing Parahydrogen. *Encycl. Magn. Reson.* **2007**, *9*, 750−770.
(28) Goodson, B. M. Advances in Magnetic Resonance: Nuclear Magnetic Resonance of Laser-Polarized Noble Gases in Molecules, Materials, and Organisms. *J. Magn. Reson.* **2002**, *155*, 157−216.
(29) Six, J. S.; Hughes-Riley, T.; Stupic, K. F.; Pavlovskaya, G. E.; Meersmann, T. Pathway to Cryogen Free Production of Hyperpolarized Krypton-83 and Xenon-129. *PLoS One* **2012**, *7*, No. e49927.
(30) Miller, K. W.; Reo, N. V.; Schoot Uiterkamp, A. J. M.; Stengle, D. P.; Stengle, T. R.; Williamson, K. L. Xenon NMR: Chemical Shifts of a General Anesthetic in Common Solvents, Proteins, and Membranes. *Proc. Natl. Acad. Sci. U. S. A.* **1981**, *78*, 4946−4949.
(31) Fraissard, J.; Ito, T. 129Xe n.m.r. Study of Adsorbed Xenon: A New Method for Studying Zeolites and Metal-Zeolites. *Zeolites* **1988**, *8*, 350−361.
(32) Ratcliffe, C. I. Xenon Nmr. *Annu. Rep. NMR Spectrosc.* **1998**, *36*, 123−221.
(33) Bonardet, J.-L.; Fraissard, J.; Gédéon, A.; Springuel-Huet, M.-A. Nuclear Magnetic Resonance of Physisorbed ^{129}Xe Used as a Probe to Investigate Porous Solids. *Catal. Rev.: Sci. Eng.* **1999**, *41*, 115−225.
(34) Kaiser, L. G.; Meersmann, T.; Logan, J. W.; Pines, A. Visualization of Gas Flow and Diffusion in Porous Media. *Proc. Natl. Acad. Sci. U. S. A.* **2000**, *97*, 2414−2418.
(35) Liu, Y.; Zhang, W.; Liu, Z.; Xu, S.; Wang, Y.; Xie, Z.; Han, X.; Bao, X. Direct Observation of the Mesopores in ZSM-5 Zeolites with Hierarchical Porous Structures by Laser-Hyperpolarized ^{129}Xe NMR. *J. Phys. Chem. C* **2008**, *112*, 15375−15381.
(36) Pavlovskaya, G.; Six, J.; Meersman, T.; Gopinathan, N.; Rigby, S. P. NMR Imaging of Low Pressure, Gas-Phase Transport in Packed Beds Using Hyperpolarized Xenon-129. *AIChE J.* **2015**, *61*, 4013−4019.
(37) Sozzani, P.; Bracco, S.; Comotti, A. Porous Materials Explored by Hyperpolarized Xenon NMR. In *Hyperpolarized Xenon-129 Magnetic Resonance: Concepts, Production, Techniques and Applications*; Meersmann, T., Brunner, E., Eds.; The Royal Society of Chemistry: Cambridge, U.K., 2015; pp 164−184.
(38) Boudart, M.; De Ménorval, L.-C.; Fraissard, J.; Valença, G. P. Study by Xenon NMR of Platinum Particles Supported on Alumina. *J. Phys. Chem.* **1988**, *92*, 4033−4035.
(39) Fraissard, J. NMR Studies of Supported Metal Catalysts. *Catal. Today* **1999**, *51*, 481−499.
(40) Bertmer, M. Solid-State NMR Studies of Small Molecule Adsorption in Metal-Organic Frameworks (MOFs). *Mod. Magn. Reson.* **2018**, 635−649.
(41) Stupic, K. F.; Six, J. S.; Olsen, M. D.; Pavlovskaya, G. E.; Meersmann, T. Combustion Resistance of the ^{129}Xe Hyperpolarized Nuclear Spin State. *Phys. Chem. Chem. Phys.* **2013**, *15*, 94−97.
(42) Rogers, N. J.; Hill-Casey, F.; Stupic, K. F.; Six, J. S.; Lesbats, C.; Rigby, S. P.; Fraissard, J.; Pavlovskaya, G. E.; Meersmann, T. Molecular Hydrogen and Catalytic Combustion in the Production of Hyperpolarized ^{83}Kr and ^{129}Xe MRI Contrast Agents. *Proc. Natl. Acad. Sci. U. S. A.* **2016**, *113*, 3164−3168.
(43) Jameson, C. J.; Jameson, A. K.; Cohen, S. M. Temperature and Density Dependence Of ^{129}Xe Chemical Shift in Xenon Gas. *J. Chem. Phys.* **1973**, *59*, 4540−4546.
(44) Peuravaara, P.; Karjalainen, J.; Zhu, J.; Mareš, J.; Lantto, P.; Vaara, J. Chemical Shift Extremum of ^{129}Xe(Aq) Reveals Details of Hydrophobic Salvation. *Sci. Rep.* **2018**, *8*, 1−11.
(45) Yuan, H.; Murad, S.; Jameson, C. J.; Olson, J. D. Molecular Dynamics Simulations of Xe Chemical Shifts and Solubility in N-Alkanes. *J. Phys. Chem. C* **2007**, *111*, 15771−15783.
(46) Bartik, K.; Luhmer, M.; Dutasta, J. P.; Collet, A.; Reisse, J. 129Xe and 1H NMR Study of the Reversible Trapping of Xenon by Cryptophane-A in Organic Solution. *J. Am. Chem. Soc.* **1998**, *120*, 784−791.
(47) Schilling, F.; Schröder, L.; Palaniappan, K. K.; Zapf, S.; Wemmer, D. E.; Pines, A. MRI Thermometry Based on Encapsulated Hyperpolarized Xenon. *ChemPhysChem* **2010**, *11*, 3529−3533.
(48) Cheung, T. T. P. Temperature Dependence of 129Xe NMR of Xenon in Microporous Solids. *J. Phys. Chem.* **1995**, *99*, 7089−7095.
(49) Labouriau, A.; Pietrass, T.; Weber, W. A.; Gates, B. C.; Earl, W. L. Temperature Dependence of Nuclear Magnetic Resonance Chemical Shifts of ^{129}Xe in the α-Cages of NaY Zeolite. *J. Phys. Chem. B* **1999**, *103*, 4323−4329.

DOI: 10.1021/acscatal.9b05000
ACS Catal. 2020, 10, 1417−1422

(50) Schröder, L. Xenon for NMR Biosensing - Inert but Alert. *Phys. Medica* **2013**, *29*, 3−16.
(51) Zhang, L.; Burant, A.; McCallister, A.; Zhao, V.; Koshlap, K. M.; Degan, S.; Antonacci, M.; Branca, R. T. Accurate MR Thermometry by Hyperpolarized ^{129}Xe. *Magn. Reson. Med.* **2017**, *78*, 1070−1079.
(52) Branca, R. T.; He, T.; Zhang, L.; Floyd, C. S.; Freeman, M.; White, C.; Burant, A. Detection of Brown Adipose Tissue and Thermogenic Activity in Mice by Hyperpolarized Xenon MRI. *Proc. Natl. Acad. Sci. U. S. A.* **2014**, *111*, 18001−18006.
(53) Antonacci, M. A.; Zhang, L.; Degan, S.; Erdmann, D.; Branca, R. T. Calibration of Methylene-Referenced Lipid-Dissolved Xenon Frequency for Absolute MR Temperature Measurements. *Magn. Reson. Med.* **2019**, *81*, 765−772.
(54) Bowers, C. R.; Weitekamp, D. P. Transformation of Symmetrization Order to Nuclear-Spin Magnetization by Chemical Reaction and Nuclear Magnetic Resonance. *Phys. Rev. Lett.* **1986**, *57*, 2645−2648.
(55) Pravica, M. G.; Weitekamp, D. P. Net NMR Alignment by Adiabatic Transport of Parahydrogen Addition Products to High Magnetic Field. *Chem. Phys. Lett.* **1988**, *145*, 255−258.
(56) Bowers, C. R.; Weitekamp, D. P. Parahydrogen and Synthesis Allow Dramatically Enhanced Nuclear Alignment. *J. Am. Chem. Soc.* **1987**, *109*, 5541−5542.
(57) Duckett, S. B.; Newell, C. L.; Eisenberg, R. Observation of New Intermediates in Hydrogenation Catalyzed by Wilkinson's Catalyst, RhCl(PPh3)3, Using Parahydrogen-Induced Polarization. *J. Am. Chem. Soc.* **1994**, *116*, 10548−10556.
(58) Colebrooke, S. A.; Duckett, S. B.; Lohman, J. A. B.; Eisenberg, R. Hydrogenation Studies Involving Halobis(Phosphine)-Rhodium(I) Dimers: Use of Parahydrogen Induced Polarisation to Detect Species Present at Low Concentration. *Chem. - Eur. J.* **2004**, *10*, 2459−2474.
(59) Salnikov, O. G.; Kovtunov, K. V.; Barskiy, D. A.; Khudorozhkov, A. K.; Inozemtseva, E. A.; Prosvirin, I. P.; Bukhtiyarov, V. I.; Koptyug, I. V. Evaluation of the Mechanism of Heterogeneous Hydrogenation of α,β-Unsaturated Carbonyl Compounds via Pairwise Hydrogen Addition. *ACS Catal.* **2014**, *4*, 2022−2028.
(60) Burueva, D. B.; Salnikov, O. G.; Kovtunov, K. V.; Romanov, A. S.; Kovtunova, L. M.; Khudorozhkov, A. K.; Bukhtiyarov, A. V.; Prosvirin, I. P.; Bukhtiyarov, V. I.; Koptyug, I. V. Hydrogenation of Unsaturated Six-Membered Cyclic Hydrocarbons Studied by the Parahydrogen-Induced Polarization Technique. *J. Phys. Chem. C* **2016**, *120*, 13541−13548.
(61) Salnikov, O. G.; Kovtunov, K. V.; Nikolaou, P.; Kovtunova, L. M.; Bukhtiyarov, V. I.; Koptyug, I. V.; Chekmenev, E. Y. Heterogeneous Parahydrogen Pairwise Addition to Cyclopropane. *ChemPhysChem* **2018**, *19*, 2621−2626.
(62) Salnikov, O. G.; Kovtunova, L. M.; Skovpin, I. V.; Bukhtiyarov, V. I.; Kovtunov, K. V.; Koptyug, I. V. Mechanistic Insight into the Heterogeneous Hydrogenation of Furan Derivatives with the Use of Parahydrogen. *ChemCatChem* **2018**, *10*, 1178−1183.
(63) Kovtunov, K. V.; Barskiy, D. A.; Coffey, A. M.; Truong, M. L.; Salnikov, O. G.; Khudorozhkov, A. K.; Inozemtseva, E. A.; Prosvirin, I. P.; Bukhtiyarov, V. I.; Waddell, K. W.; Chekmenev, E. Y.; Koptyug, I. V. High-Resolution 3D Proton MRI of Hyperpolarized Gas Enabled by Parahydrogen and Rh/TiO_2 Heterogeneous Catalyst. *Chem. - Eur. J.* **2014**, *20*, 11636−11639.
(64) Kovtunov, K. V.; Romanov, A. S.; Salnikov, O. G.; Barskiy, D. A.; Chekmenev, E. Y.; Koptyug, I. V. Gas Phase UTE MRI of Propane and Propene. *Tomography* **2016**, *2*, 49−55.
(65) Burueva, D. B.; Kovtunov, K. V.; Bukhtiyarov, A. V.; Barskiy, D. A.; Prosvirin, I. P.; Mashkovsky, I. S.; Baeva, G. N.; Bukhtiyarov, V. I.; Stakheev, A. Y.; Koptyug, I. V. Selective Single-Site Pd-In Hydrogenation Catalyst for Production of Enhanced Magnetic Resonance Signals Using Parahydrogen. *Chem. - Eur. J.* **2018**, *24*, 2547−2553.
(66) Kovtunov, K. V.; Lebedev, D.; Svyatova, A.; Pokochueva, E. V.; Prosvirin, I. P.; Gerasimov, E. Y.; Bukhtiyarov, V. I.; Müller, C. R.; Fedorov, A.; Koptyug, I. V. Robust In Situ Magnetic Resonance Imaging of Heterogeneous Catalytic Hydrogenation with and without Hyperpolarization. *ChemCatChem* **2018**, *11*, 969−973.
(67) Filimonova, S. V.; Mastikhin, V. M.; Smolikov, M. D.; Belyi, S. S.; Duplyakin, V. K. ^{129}Xe Nuclear Magnetic Resonance Studies of Supported Platinum-Alumina Catalysts. *React. Kinet. Catal. Lett.* **1992**, *48*, 209−216.
(68) Tyler, D. J.; Robson, M. D.; Henkelman, R. M.; Young, I. R.; Bydder, G. M. Magnetic Resonance Imaging with Ultrashort TE (UTE) PULSE Sequences: Technical Considerations. *J. Magn. Reson. Imaging* **2007**, *25*, 279−289.

DOI: 10.1021/acscatal.9b05000
ACS Catal. 2020, 10, 1417−1422